Systematic study of the break-up fusion process in the ^{12}C + ^{165}Ho system and interplay of entrance channel parameters

Suhail A. Tali ,[1,*] Harish Kumar,[1] M. Afzal Ansari,[1,†] Asif Ali,[1] D. Singh,[2] Rahbar Ali,[3] Pankaj K. Giri,[2]
Sneha B. Linda,[2] R. Kumar,[4] Siddharth Parashari,[1] S. Muralithar,[4] and R. P. Singh[4]

[1]*Department of Physics, Aligarh Muslim University, Aligarh-202002, India*
[2]*Centre for Applied Physics, Central University of Jharkhand, Ranchi-835205, India*
[3]*Department of Physics, G.F. (P.G.) College Shahjahanpur-242001, India*
[4]*Inter-University Accelerator Centre, New Delhi-110067, India*

To understand the low-energy incomplete fusion (ICF) reaction dynamics, the excitation function measurements of ^{12}C + ^{165}Ho system has been performed in the energy region of $\approx$ 4–7 MeV/nucleon, by employing the stacked foil activation technique. The cross sections of the measured evaporation residues are compared with the theoretical predictions of statistical model code PACE4, which takes into account only the complete fusion (CF) reaction cross section. It is observed that residues populated via xn and pxn channels are in good agreement with the PACE4 predictions, implying that these residues are populated via CF process. However, in the case of α-emission channels a significant enhancement from the PACE4 predictions is observed even after the deduction of precursor contribution, which is accredited to ICF process. The projectile break-up probability is found to increase with increment in the incident projectile energy. Further, the dependence of incomplete fusion dynamics on entrance channel parameters like mass asymmetry, Coulomb effect ($Z_P Z_T$), and projectile Q_α value is systematically studied. The present results reveal that a single entrance channel parameter does not oversee the ICF reaction dynamics but have varying contributions depending upon the projectile-target combination. Moreover, the effect of projectile break-up on complete fusion cross section at energies above the Coulomb barrier is also studied. The suppression in fusion cross section is observed when compared with the universal fusion function.

I. INTRODUCTION

Fusion reactions induced by heavy ions (HIs) play an utmost role in nuclear physics, as they enable us to study the properties of super-heavy nuclei near and away from the stability line. At projectile energies above the Coulomb barrier, complete fusion (CF) and incomplete fusion (ICF) are the two most dominant reaction modes [1–3]. Study of such fusion reactions has remained the subject of great interest for both theoretical and experimental nuclear physicists over the past two decades. In the case of CF, the incident projectile completely fuses with the target nucleus and leads to the formation of highly excited compound nucleus (CN), which de-excites via emission of light nuclear particles and γ rays. In ICF (also known as break-up fusion process), the incident projectile breaks in the vicinity of target nuclear field, one of the fragment fuses with the target nucleus giving rise to a composite system of low mass, excitation energy, charge, and momentum transfer. The excited composite system also de-excites via emission of light nuclear particles and γ rays. The unfused fragment moves as a spectator in the forward direction, with nearly the projectile velocity and have no impact

on the way the reaction proceeds [4,5]. Semiclassically, the CF and ICF phenomenon in heavy-ion (HI) interactions can be explained on the basis of driving input angular momentum (ℓ) imparted into the system [2,3,6]. For the values, with $\ell < \ell_{\text{crit}}$, there is a pocket in an effective potential energy curve, (the attractive nuclear potential dominates the sum of repulsive Coulomb and centrifugal potential) hence the incident projectile is completely assimilated by the target nucleus-CF. However as the energy of incident projectile increases $\ell > \ell_{\text{crit}}$, the fusion pocket in the effective potential energy curve subsequently vanishes, hence to provide the sustainable amount of input ℓ, the incident projectile breaks into clusters, leading to the fusion of one of the fragment with the target nucleus-ICF [1–3]. Some studies have also reported the existence of ICF well below the ℓ_{crit} [7–10]. To understand the phenomenon of ICF reaction dynamics various theoretical models have been put forth, but none of them is able to reproduce satisfactorily the experimentally measured ICF data below 8 MeV/nucleon [3,5,7], this has revived the interest in exploring the low-energy ICF reaction dynamics. The another unresolved question which is also of large interest is to understand the systematic dependence of ICF on various entrance channel parameters such as projectile energy, mass asymmetry, Coulomb effect ($Z_P Z_T$), projectile structure, and input ℓ values. In the present work, with an incentive to comprehend the systematic dependence of ICF on

*amusuhailtali@gmail.com
†drmafzalansari@yahoomail.com

various entrance channel parameters, the excitation function (EFs) measurements of evaporation residues populated in the interaction of $^{12}C + ^{165}Ho$ system have been measured in the energy ranging from $\approx$ 4–7 MeV/nucleon. The experimentally measured cross sections of the evaporation residues have been compared with the fusion evaporation code PACE4 [11].

It is important to mention that Gupta *et al.* [12] have also studied the same projectile-target system, but the EF measurements of the evaporation residues (ERs) reported has been studied only at four energy points and no ICF fraction has been deduced. Moreover the authors have limited their study up to comparing the experimentally measured cross sections with the fusion evaporation codes ALICE-91 and CASCADE. In view of this, the better presentation of the EF measurements of the ERs, the behavior of ICF with the incident projectile energy and other entrance channel parameters is reported in the present work. A few of the data points from EF measurements of Ref. [12] agree with our work. The EFs of the ERs ^{171}Ta (6n), ^{172}Lu (αn), ^{170}Lu ($\alpha 3n$), ^{169}Yb ($\alpha p3n$), and ^{166}Tm ($2\alpha 3n$) are reported for the first time; however, we could not observe the ERs like ^{167}Lu ($\alpha 6n$) and ^{165}Tm ($2\alpha 4n$). Further, the present work provides the EF measurement of ERs at additional energy points in a more systematic manner and ICF dependence on various entrance channel parameters, including a large number of projectile-target combinations to investigate the possible aspects of ICF reaction dynamics in the energy region of $\approx$ 4–7 MeV/nucleon. It is also important to mention here that the value of ICF fraction F_{ICF} (%) that we have reported for the $^{12}C + ^{165}Ho$ system [12] in Ref. [5] was actually taken from Refs. [6,13]. However, in the present work we observe that while comparing our data with that of Ref. [12], the F_{ICF} (%) that actually comes from the work of Gupta *et al.* [12] is much larger than reported in Refs. [6,13], which mostly seems to be due to the unexpected cross sections of ^{165}Tm ($2\alpha 4n$) reported in Ref. [12]. Moreover, an attempt has been made to understand the projectile break-up effects on the CF cross sections at projectile energies above the Coulomb barrier, the universal fusion function (UFF) [14,15] is used as a standard reference.

II. EXPERIMENTAL PROCEDURE

The 15UD Pelletron accelerator facilities at Inter-University Accelerator Centre (IUAC), New Delhi, India, were used to carry out the present experiment. The experimental procedure is similar to our earlier work [5,8], however a brief description is given here. Two stacks, each comprising of four ^{165}Ho target foils backed by aluminum foils (Al-foils served as catcher as well as energy degrader), were bombarded by ^{12}C (alpha clustered) Ion beam at incident projectile energies 88 and 71 MeV, respectively. The ^{165}Ho target foils (purity >99.9%) of thickness ranging from 1.0 to 1.5 mg/cm^2 and aluminum foils of thickness ranging from 1.5 to 2.0 mg/cm^2 were prepared at Target Development Laboratory IUAC, New Delhi, by employing the rolling technique. To minimize the error in thickness measurement, both ^{165}Ho target foils as well as aluminum foil thicknesses were determined by using the microbalance as well as α-transmission method. Keeping the half-lives of interested ERs

into consideration, the two stacks were separately irradiated for about seven hours in the general purpose scattering chamber (GPSC), which is provided with an in-vacuum transfer facility to minimize the time lapse between the stop of irradiation and start of counting. The target ladder was immediately dismounted when the beam was stopped and the activities induced in the samples were recorded using the precalibrated high purity Germanium (HPGe) detector coupled to a computer automated measurement and control (CAMAC) based data acquisition system CANDLE [16] software. The HPGe detector used in the present experiment was pre-calibrated using the standard ^{152}Eu source of known initial strength. The energy resolution of the HPGe detector was found to be 2.5 keV for 1408 keV γ ray of standard ^{152}Eu source.

III. ANALYSIS AND EXPERIMENTAL RESULTS

The recorded γ-ray spectra obtained at various energy points and at different source to detector positions were analyzed using the CANDLE [16] software. The cross section (σ) of the ERs populated in the interaction of $^{12}C + ^{165}Ho$ system, in the energy region of 57–88 MeV, were calculated using the following expression [5]:

$$\sigma(E) = \frac{A\lambda \exp(\lambda t_2)}{N_0 \phi I_\gamma K \varepsilon_G [1 - \exp(-\lambda t_1)][1 - \exp(-\lambda t_3)]}, \quad (1)$$

where A is the total number of counts under the photopeak of any characteristic γ ray, λ is the decay constant of particular ER, t_2 is the time period between beam stop time and counting start time, N_0 is the initial number of nuclei present in the irradiated target foil, ϕ is the incident beam flux, I_γ is the branching ratio of the characteristic γ ray, $K = [\{1 - \exp(-\mu d)\}/\mu d]$ is the self-absorption correction factor, for the target material of thickness "d" and absorption coefficient "μ," ε_G is the geometry-dependent efficiency of the detector, t_1 is the irradiation time, and t_3 is the spectra recording time. A C++ program EXPSIGMA based on this formulation has been used for computing the cross section of the ERs. The populated ERs were initially identified by their characteristic γ rays and finally confirmed by the decay curve analysis. The γ ray spectra recorded at $E_{lab} = 70.38 \pm 0.62$ MeV are shown in Fig. 1. It is important to mention that most of the ERs populated via emission of α and 2α emission channels have half-lives in days, hence Fig. 1(b) is the recorded γ-ray spectra at large lapse time at the same incident projectile energy ($E_{lab} = 70.38 \pm 0.62$ MeV). As a representative case the decay curve analysis of the ERs, ^{171}Ta, ^{170}Lu, and ^{169}Yb having half-lives of 23.3 min, 2.01 days, and 32.03 days, respectively, are shown in Fig. 2. These half-life plots correspond to the beam energy at 87.38 ± 0.62 MeV. Moreover, different γ-ray peaks have been assigned to the respective ERs populated through CF and/or ICF reaction channels. The list of all identified ERs, their half-lives, and other spectroscopic properties are tabulated in Table I. It is also significant to mention that ERs populated through a specific channel in its excited state quite often de-excite via emission of γ rays of different energies. Hence, the reported values of cross sections for most of the ERs are the weighted
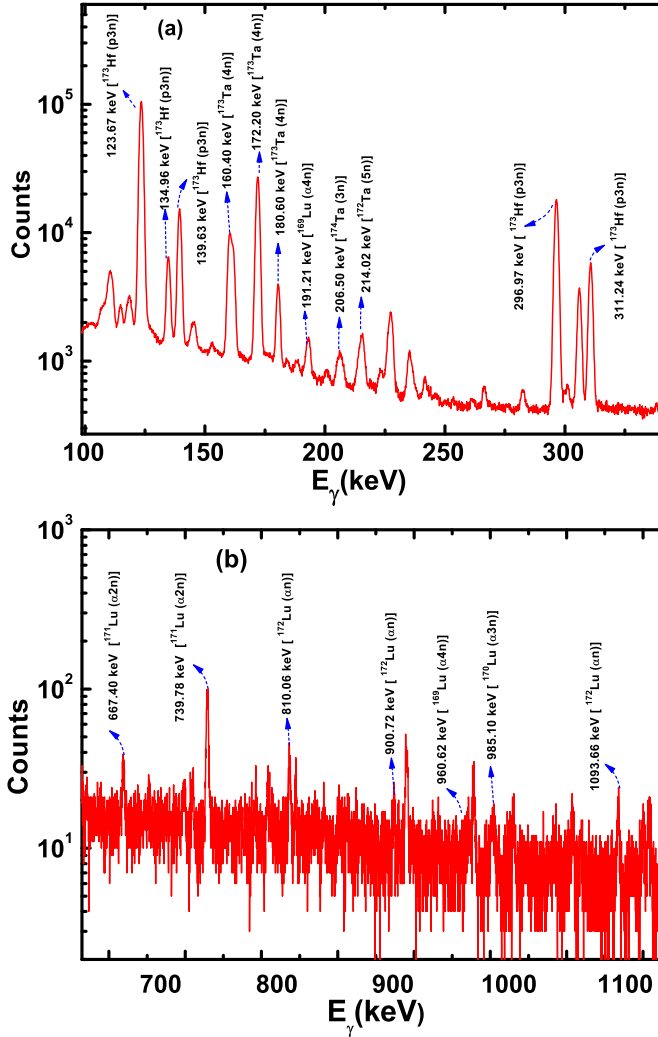
FIG. 1. Typical γ-ray energy spectra obtained from the interactions of ^{12}C + ^{165}Ho system at $E_{\text{lab}} = 70.38 \pm 0.62$ MeV energy. Some of the identified γ-ray peaks have been assigned to respective evaporation residues populated via CF and/or ICF channels.

average of individual cross sections obtained for different characteristic γ rays [17].

The experimentally measured cross sections of the ERs along with the errors are given in Tables II and III. The error in the measured cross sections of the ERs may arise because of (i) the lack of uniformity in the thickness of target foils and an imprecise measurement of the target foil thickness may lead to the uncertainty in calculating the number of target nuclei. The thickness of each target foil was measured at various positions by α-transmission method to minimize the error that may arise due to target nonuniformity. Presently, the error in the thickness of target foils comes out to be <3%. (ii) The instability in the beam current may result in the variation of incident flux (ϕ). Proper care was taken to keep the beam current constant and error due to beam fluctuation is estimated to be <6%. (iii) The uncertainty in the determination of geometry dependent efficiency may also add to the error in the measured cross sections. This is due to the

statistical fluctuation in the counts under the peak and it was observed to be <5%. (iv) The dead time of the spectrometer may also lead to the error. The dead time was kept <10% by adjusting the distance between the irradiated foils and the detector. Apart from the uncertainties in the decay constant and branching ratio, the overall errors including statistical errors in the present measurements is estimated to be ⩽15%.

A. Estimation of independent cross sections

In the present work, the excitation function (EF) of 13 ERs has been measured. The ERs are identified on the basis of their characteristic γ rays and half-lives. It is observed that some of the ERs (^{174}Ta, ^{173}Ta, ^{172}Ta, ^{171}Ta, ^{172}Lu, ^{170}Lu, ^{169}Lu, ^{167}Tm, and ^{166}Tm) are populated independently in the interaction of ^{12}C with ^{165}Ho and give rise to independent cross sections. A few of the ERs (^{173}Hf, ^{171}Hf, ^{171}Lu, and ^{169}Yb) are strongly fed by their higher charge precursor isobars through an electron capture (EC) process and/or β^+ emission and hence gives rise to the cumulative cross section in addition to their direct production. In these cases, by using the Cavinato et al. [18] formalism the independent cross section has been evaluated using the following expressions:

$$\sigma_{\text{ind}}^{\text{exp}}(^{173}\text{Hf}) = \sigma_{\text{cum}}^{\text{exp}}(^{173}\text{Hf}) - 1.153\,\sigma_{\text{ind}}^{\text{exp}}(^{173}\text{Ta}), \quad (2)$$

$$\sigma_{\text{ind}}^{\text{exp}}(^{171}\text{Hf}) = \sigma_{\text{cum}}^{\text{exp}}(^{171}\text{Hf}) - 1.033\,\sigma_{\text{ind}}^{\text{exp}}(^{171}\text{Ta}), \quad (3)$$

$$\sigma_{\text{ind}}^{\text{exp}}(^{171}\text{Lu}) = \sigma_{\text{cum}}^{\text{exp}}(^{171}\text{Lu}) - 1.065\,\sigma_{\text{ind}}^{\text{exp}}(^{171}\text{Hf})$$
$$- 1.068\,\sigma_{\text{ind}}^{\text{exp}}(^{171}\text{Ta}), \quad (4)$$

$$\sigma_{\text{ind}}^{\text{exp}}(^{169}\text{Yb}) = \sigma_{\text{cum}}^{\text{exp}}(^{169}\text{Yb}) - 1.046\,\sigma_{\text{ind}}^{\text{exp}}(^{169}\text{Lu}). \quad (5)$$

B. Excitation function measurements of the xn and pxn emission channels in the framework of fusion-evaporation code PACE4

The experimentally measured cross section of the ERs populated by the de-excitation of the CN formed via CF of the incident projectile with the target nucleus should be reproduced by the fusion-evaporation code PACE4 [11]. This code determines only the CF cross section of the ERs, using the Bass formula [19]. The enhancement, if any, in the measured cross sections from the predictions of PACE4 code will provide information about the different reaction mechanism involved in the formation of ERs. PACE4 is a statistical model code, based on the Hauser-Feshbach theory of CN decay [20]. During the de-excitation of CN, the angular momentum projections are deduced at each level, which in-turn makes it possible to calculate the angular distribution of the ERs. The transmission coefficient for light emitted particles like neutron (n), proton (p), and alpha (α) are calculated using the optical model potentials [21]. The Gilbert and Cameron's level density parameter value was used during the calculation [22]. The level density parameter ($a = A/K$ MeV^{-1}, where "A" is the mass number of the CN and "K" is a free parameter) is one of the important parameter in PACE4 code. The value of "K" may be varied within the physically justified limits to reproduce the experimentally measured cross sections of the
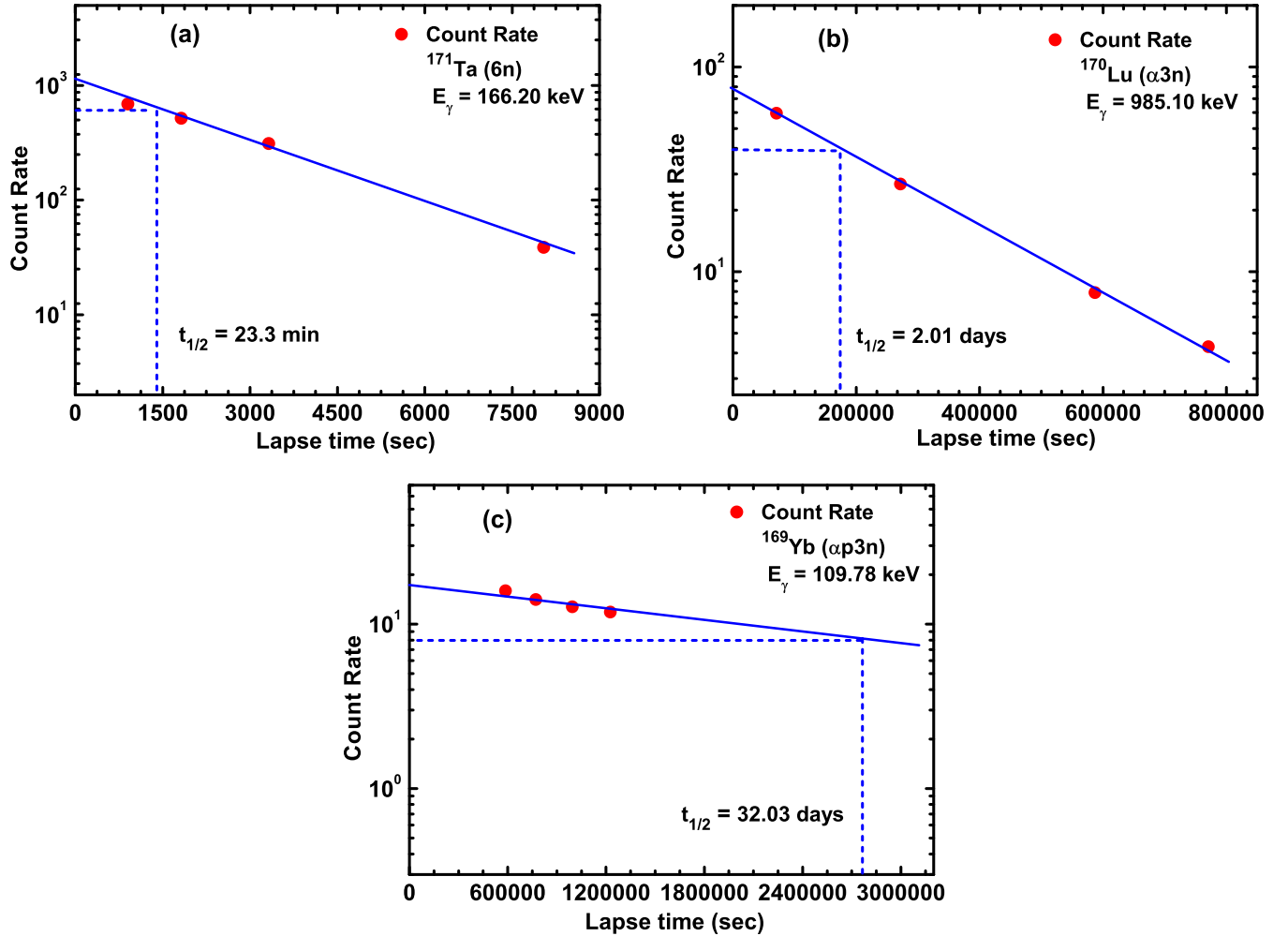
FIG. 2. Experimentally observed decay curves of (a) ^{171}Ta (23.3 min), (b) ^{170}Lu (2.01 days), and (c) ^{169}Yb (32.03 days) populated via 6n, α3n, and αp3n channels, respectively, in the interaction of ^{12}C + ^{165}Ho system.

ERs [23]. Most of the parameters in the input file of PACE4 code have been used as default values except the charge, mass and spin of the projectile and target.

To understand the reaction mechanism involved and to look for the right choice of level density parameter, the EF of the ERs ^{174}Ta, ^{173}Ta, ^{172}Ta, ^{171}Ta, ^{173}Hf, and ^{171}Hf populated by the emission of 3n, 4n, 5n, 6n, p3n, and p5n channels, respectively, are shown in Figs. 3 and 4. The experimentally measured cross sections have been compared with the theoretical predictions of PACE4 at different level density parameters "*a*" by varying the free parameter from $K = 8$ to 10. These ERs are identified on the basis of their characteristic γ-rays and finally confirmed by the decay curve analysis. It may be seen from Fig. 3 that the experimentally measured cross sections of ERs ^{174}Ta, ^{173}Ta, ^{172}Ta, and ^{171}Ta match well with the theoretical predictions of PACE4 for level density parameter $a = A/10 \, \text{MeV}^{-1}$, which infers that these ERs are populated by CF process only. Moreover, during the decay curve analysis, it was observed that the ERs ^{173}Hf and ^{171}Hf are strongly fed from their higher charge precursor isobars ^{173}Ta and ^{171}Ta, respectively, through an electron capture (EC)

process and/or β^+ emission. The independent cross section of ^{173}Hf ($\sigma^{\text{ind }173}$Hf) and ^{171}Hf ($\sigma^{\text{ind }171}$Hf) have been calculated using the Cavinato *et al.* [18] formalism by employing expressions 2 and 3, respectively. As shown in Fig. 4, the independent cross sections of both these ERs are in good agreement with the predictions of PACE4 code at $K = 10$, indicating that these residues are also populated via de-excitation of fully equilibrated CN ^{177}Ta*, i.e., by CF of incident projectile (^{12}C) with target nucleus (^{165}Ho). Furthermore, the experimentally measured cross sections of the identified ERs reported in Ref. [12] are also depicted in Figs. 3 and 4 and few of the data points are found to be consistent with the present data measurements.

In Fig. 5, the sum of experimentally measured cross sections of ERs populated via xn and pxn channels ($\Sigma\sigma^{\text{exp}}_{\text{xn+pxn}}$) have been compared with that predicted by PACE4 code ($\Sigma\sigma^{\text{PACE4}}_{\text{xn+pxn}}$) for the same ERs at free parameter value $K = 10$. It may be observed from this figure that the theoretical calculations of PACE4 code significantly reproduce the sum of experimentally measured cross sections. This once again suggests that the ERs ^{174}Ta, ^{173}Ta, ^{172}Ta, ^{171}Ta, ^{173}Hf, and

TABLE I. List of identified evaporation residues populated in ^{12}C + ^{165}Ho system via CF and/or ICF, along with their spectroscopic properties.

Reactions	Residues	$T^{1/2}$	J^π	E_γ (keV)	I_γ (%)
^{165}Ho (^{12}C, 3n)	^{174}Ta	1.05 h	3^+	206.50	58.0
				764.79	1.3
				971.06	1.2
^{165}Ho (^{12}C, 4n)	^{173}Ta	3.14 h	$5/2^-$	160.40	4.9
				172.20	18
				180.60	2.2
^{165}Ho (^{12}C, 5n)	^{172}Ta	36.8 min	3^+	214.02	55
				1085.58	8.1
				1109.27	14.9
^{165}Ho (^{12}C, 6n)	^{171}Ta	23.3 min	$5/2^-$	166.20	19.2[a]
				175.40	16.0[a]
				501.80	22.6[a]
				506.40	54.0[a]
^{165}Ho (^{12}C, p3n)	^{173}Hf	23.6 h	$1/2^-$	123.67	83
				139.63	12.7
				296.97	33.9
				311.24	10.7
^{165}Ho (^{12}C, p5n)	^{171}Hf	12.1 h	$7/2^+$	469.30	100[a]
				662.20	266[a]
				1071.81	148[a]
^{165}Ho (^{12}C, αn)	^{172}Lu	6.7 d	4^-	810.06	16.6
				900.72	29.8
				1093.66	62.5
^{165}Ho (^{12}C, α2n)	^{171}Lu	8.24 d	$7/2^+$	667.40	11.1
				739.78	47.8
^{165}Ho (^{12}C, α3n)	^{170}Lu	2.01 d	0^+	193.13	2.1
				985.10	5.5
^{165}Ho (^{12}C, α4n)	^{169}Lu	34.06 h	$7/2^+$	191.21	20.6
				960.62	23.4
^{165}Ho (^{12}C, αp3n)	^{169}Yb	32.03 d	$7/2^+$	109.78	17.5
^{165}Ho (^{12}C, 2α2n)	^{167}Tm	9.25 d	$1/2^+$	207.80	41
^{165}Ho (^{12}C, 2α3n)	^{166}Tm	7.70 h	2^+	705.33	11.0
				778.82	18.9

[a]The relative intensities of the γ rays.

^{171}Hf are populated by the CF of incident projectile (^{12}C) with the target nucleus (^{165}Ho). Hence, the choice of the input parameters used in the analysis of ERs populated by the emission of xn and pxn channels can be used consistently as a fixed parameter for carrying out the analysis of all the ERs populated by the α and 2α emission channels and any enhancement from the theoretical predictions may be accredited to ICF process as proposed by several recent studies [2,5].

C. Excitation function measurements of the αxn, αpxn and 2αxn emission channels: Accountable for ICF cross section

The EF measurements of seven ERs populated via αxn, αpxn, and 2αxn emission channels, namely, ^{172}Lu (αn), ^{171}Lu (α2n), ^{170}Lu (α3n), ^{169}Lu (α4n), ^{169}Yb (αp3n), ^{167}Tm (2α2n), and ^{166}Tm (2α3n) are shown in Figs. 6 and 7. The experimentally measured cross sections for these ERs have been compared with the theoretical predictions of PACE4 code at level density parameter $a = A/10\,\mathrm{MeV}^{-1}$, represented by the solid blue curves. It can be seen from these graphs that the experimentally measured cross sections show a significant enhancement from the PACE4 predictions. As mentioned earlier, that PACE4 code gives only the CF cross sections and does not take ICF cross section into account, hence this enhancement is attributed to ICF process. This implies that these ERs are populated by ICF process in addition to CF. Furthermore, the experimentally measured cross sections of the α and 2α emission ERs reported in Ref. [12] are also depicted in Figs. 6 and 7 and here also few of the data points are found to be consistent with the present data measurements.

It is also important to mention that the experimentally measured cross sections for the ERs ^{171}Lu ($t_{1/2} = 8.24$ d) populated through the emission of α2n channel has contribution in its cross section at the higher energy side, coming from the decay of higher charge precursor isobars ^{171}Ta ($t_{1/2} = 23.3$ min) and ^{171}Hf ($t_{1/2} = 12.1$h). The independent cross section has been calculated using the Cavinato *et al.* [18] formalism and expression for precursor subtraction is given by Eq. (4). Also, in the case of ^{169}Yb ($t_{1/2} = 32.03$ d) populated through the emission of αp3n channel, there is a contribution from the decay of its higher charge precursor ^{169}Lu ($t_{1/2} = 34.06$ h), the independent cross sections has been evaluated using the Eq. (5). Hence, Figs. 6(b) and 7(a) represent the independent cross sections of the ERs ^{171}Lu and ^{169}Yb, respectively. Moreover, no

TABLE II. Experimentally measured production cross sections of the evaporation residues ^{174}Ta, ^{173}Ta, ^{172}Ta, ^{171}Ta, ^{173}Hf, and ^{171}Hf populated in ^{12}C + ^{165}Ho system.

Lab Energy (MeV)	σ (^{174}Ta) (mb)	σ (^{173}Ta) (mb)	σ (^{172}Ta) (mb)	σ (^{171}Ta) (mb)	σ^{ind} (^{173}Hf) (mb)	σ^{ind} (^{171}Hf) (mb)
57.39 ± 0.66	164.77 ± 21.26	80.22 ± 9.05	–	–	0.38 ± 0.05	–
61.78 ± 0.52	108.17 ± 11.39	352.27 ± 36.97	–	–	5.72 ± 0.80	–
66.13 ± 0.52	44.06 ± 5.58	588.55 ± 77.44	7.48 ± 1.26	–	21.42 ± 2.52	–
70.38 ± 0.62	13.83 ± 1.60	590.27 ± 70.85	166.83 ± 17.08	–	30.45 ± 3.30	–
74.59 ± 0.41	3.81 ± 0.42	367.75 ± 44.78	460.0 ± 52.30	–	34.10 ± 4.36	–
78.88 ± 0.54	0.84 ± 0.10	183.05 ± 20.42	725.82 ± 73.16	24.84 ± 2.83	18.21 ± 1.90	0.34 ± 0.05
83.05 ± 0.64	0.4 ± 0.06	74.68 ± 8.01	769.45 ± 93.42	146.15 ± 17.92	11.73 ± 1.69	5.72 ± 0.70
87.38 ± 0.62	–	22.24 ± 2.68	581.56 ± 62	436.6 ± 55.03	3.92 ± 0.43	37.7 ± 3.94

TABLE III. Experimentally measured production cross sections of the evaporation residues ^{172}Lu, ^{171}Lu, ^{170}Lu, ^{169}Lu, ^{169}Yb, ^{167}Tm, and ^{166}Tm populated in ^{12}C + ^{165}Ho system.

Lab Energy (MeV)	$\sigma(^{172}$Lu) (mb)	$\sigma^{ind}(^{171}$Lu) (mb)	$\sigma(^{170}$Lu) (mb)	$\sigma(^{169}$Lu) (mb)	$\sigma^{ind}(^{169}$Yb) (mb)	$\sigma(^{167}$Tm) (mb)	$\sigma(^{166}$Tm) (mb)
57.39 ± 0.66	–	12.95 ± 1.30	4.5 ± 0.53	–	–	–	–
61.78 ± 0.52	–	23.6 ± 2.60	15.15 ± 1.70	1.73 ± 0.25	4.26 ± 0.43	7.56 ± 0.90	–
66.13 ± 0.52	–	20.11 ± 2.4	48.71 ± 4.98	4.21 ± 0.51	4.49 ± 0.45	13.37 ± 1.64	3.62 ± 0.44
70.38 ± 0.62	3.24 ± 0.33	22.51 ± 2.0	70.95 ± 7.50	17.79 ± 1.86	5.93 ± 0.60	24.34 ± 2.78	8.2 ± 0.87
74.59 ± 0.41	4.24 ± 0.42	23.76 ± 3.20	77.84 ± 8.90	54.66 ± 6.40	8.07 ± 0.90	27.93 ± 3.37	10.63 ± 0.98
78.88 ± 0.54	5.06 ± 0.60	27.96 ± 2.90	81.79 ± 7.80	90.65 ± 9.81	11.28 ± 1.30	31.07 ± 3.40	13.96 ± 1.42
83.05 ± 0.64	5.97 ± 0.62	50.30 ± 4.94	67.77 ± 7.94	121.18 ± 12.52	18.59 ± 1.90	27.8 ± 2.98	20.66 ± 2.06
87.38 ± 0.62	3.29 ± 0.44	63.69 ± 8.34	42.73 ± 4.30	168.03 ± 15.71	29.50 ± 3.15	20.2 ± 2.52	18.31 ± 1.89

contribution from any higher charge isobar was observed in any other α or 2α emission channels, hence their experimentally measured cross sections are independent in nature. The

reaction mechanism involved in the formation of ERs populated through α and 2α emission channels may be represented as;
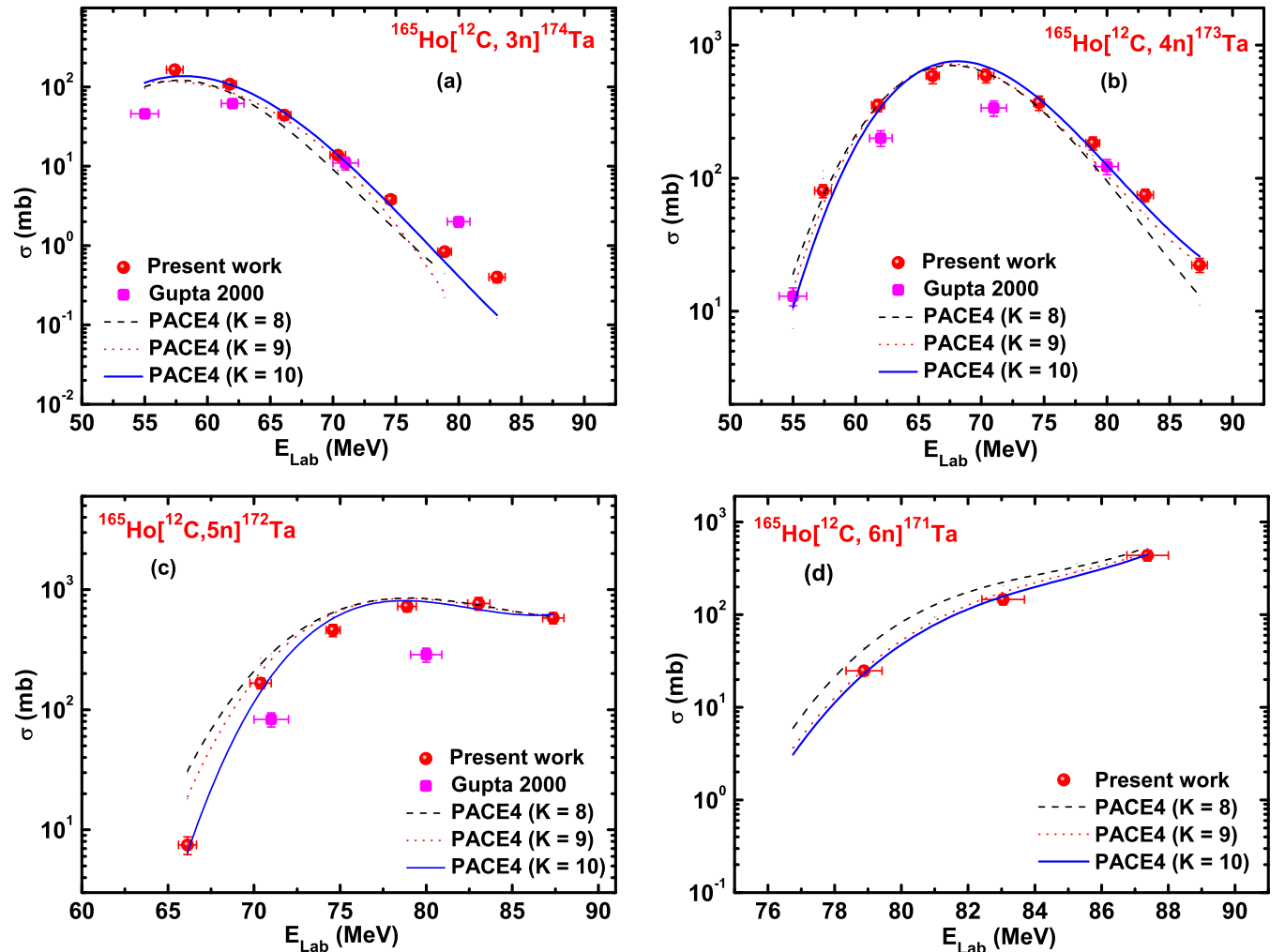

FIG. 3. Comparison of experimentally measured EFs of the ERs ^{174}Ta, ^{173}Ta, ^{172}Ta, and ^{171}Ta populated via 3n, 4n, 5n, and 6n channels, respectively, with theoretical predictions by statistical model code PACE4 for $K = 8, 9, 10$.
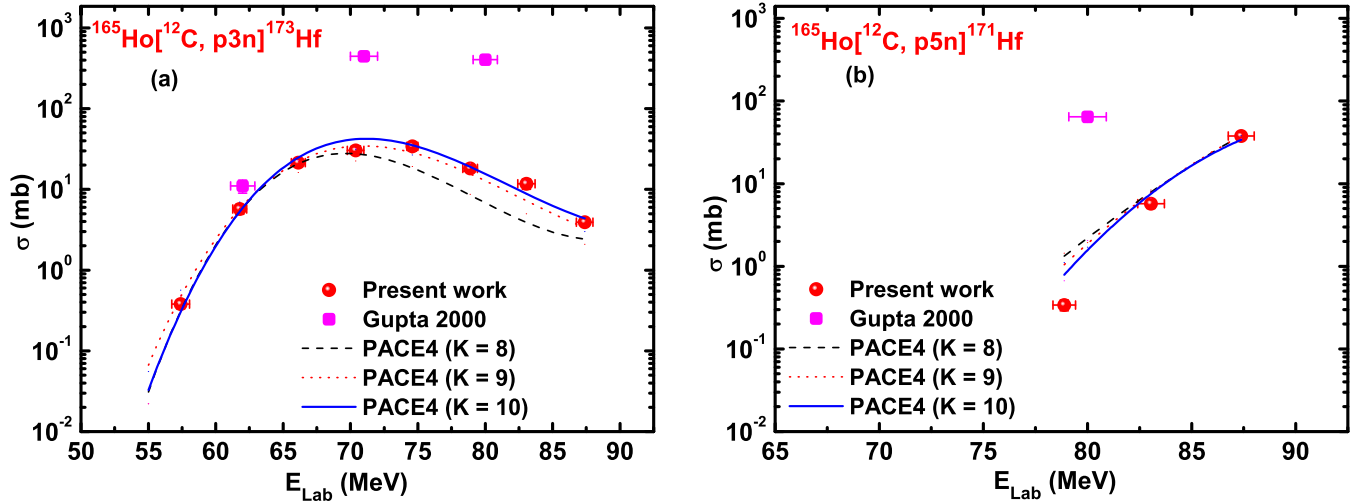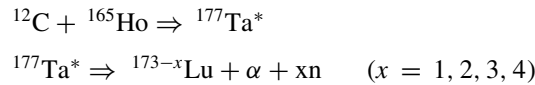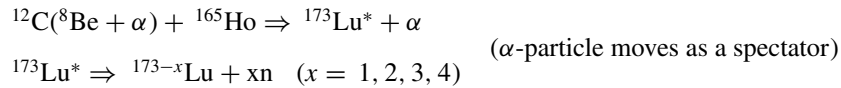
FIG. 4. Comparison of experimentally measured EFs of the ERs ^{173}Hf and ^{171}Hf populated via p3n and p5n channels, respectively, with theoretical predictions by statistical model code PACE4 for $K = 8, 9, 10$.

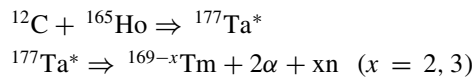1α-emission case:

(i) CF of ^{12}C with ^{165}Ho, i.e.,

$$^{12}\text{C} + {}^{165}\text{Ho} \Rightarrow {}^{177}\text{Ta}^*$$
$$^{177}\text{Ta}^* \Rightarrow {}^{173-x}\text{Lu} + \alpha + \text{xn} \quad (x = 1, 2, 3, 4)$$

(ii) ICF of ^{12}C with ^{165}Ho, i.e.,

$$^{12}\text{C}(^8\text{Be} + \alpha) + {}^{165}\text{Ho} \Rightarrow {}^{173}\text{Lu}^* + \alpha$$
$$^{173}\text{Lu}^* \Rightarrow {}^{173-x}\text{Lu} + \text{xn} \quad (x = 1, 2, 3, 4)$$
      (α-particle moves as a spectator)

2α-emission case:

(i) CF of ^{12}C with ^{165}Ho, i.e.,

$$^{12}\text{C} + {}^{165}\text{Ho} \Rightarrow {}^{177}\text{Ta}^*$$
$$^{177}\text{Ta}^* \Rightarrow {}^{169-x}\text{Tm} + 2\alpha + \text{xn} \quad (x = 2, 3)$$

(ii) ICF of ^{12}C with ^{165}Ho, i.e.,

$$^{12}\text{C}(^8\text{Be} + {}^4\text{He}) + {}^{165}\text{Ho} \Rightarrow {}^{169}\text{Tm}^* + {}^8\text{Be}$$
$$^{169}\text{Tm}^* \Rightarrow {}^{169-x}\text{Tm} + \text{xn} \quad (x = 2, 3)$$
      (^{8}Be moves as spectator)
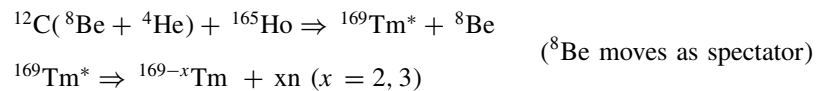
To understand the contribution of ICF or break-up fusion more clearly, the summation of independently measured experimental cross sections of all αxn, αpxn, and 2αxn emission channels ($\sum \sigma_{\alpha xn + \alpha pxn + 2\alpha xn}^{\exp}$) is compared with that evaluated by statistical model code PACE4 ($\sum \sigma_{\alpha xn + \alpha pxn + 2\alpha xn}^{\text{PACE4}}$) and shown in Fig. 8(a). It may be seen from this graph, that

the measured cross sections significantly underestimate the PACE4 predictions for the same value of level density parameter ($a = A/10 \, \text{MeV}^{-1}$). This again implies the population of these ERs via ICF along with CF. Moreover the summation of independently measured cross sections obtained from Ref. [12] is inconsistent with our measurements.
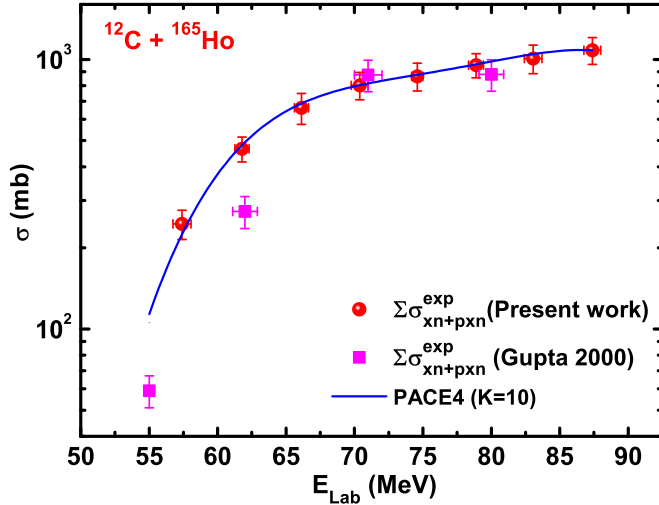
FIG. 5. Sum of experimentally measured EFs of all xn and pxn channels ($\sum \sigma_{xn+pxn}^{exp}$) are compared with that predicted by statistical model code PACE4 ($\sum \sigma_{xn+pxn}^{PACE4}$) at $K = 10$.

IV. ICF FRACTION AND INTERPLAY OF ENTRANCE CHANNEL PARAMETERS

To comprehend the dependence of ICF on various entrance channel parameters, the ICF fraction F_{ICF} (%) was deduced in the following manner:

$$F_{ICF}(\%) = \frac{\sum \sigma_{ICF}}{\Sigma\sigma_{CF} + \Sigma\sigma_{ICF}} \times 100, \qquad (6)$$

where $\sum \sigma_{ICF}$ is the sum of ICF cross section of measured α-emission channels and $\Sigma\sigma_{CF}$ is the sum of CF cross sections of all xn, pxn, αxn, αpxn, and 2αxn channels. The sum of ICF cross section of the αxn, αpxn, and 2αxn ERs was calculated by implying the same procedure ($\Sigma\sigma_{ICF} = \sum \sigma_{\alpha xn+\alpha pxn+2\alpha xn}^{exp} - \sum \sigma_{\alpha xn+\alpha pxn+2\alpha xn}^{PACE4}$) as used in Ref. [5]. It is worth mentioning here that the employed OFF-LINE activation technique has the limitation for shorter half-life channels. In the present analysis, the values of statistical model code PACE4 have been included in the unmeasured CF channels for the extraction of $\Sigma\sigma_{CF}$. However, in the evaluation of $\Sigma\sigma_{ICF}$ no correction has been made to incorporate the unmeasured
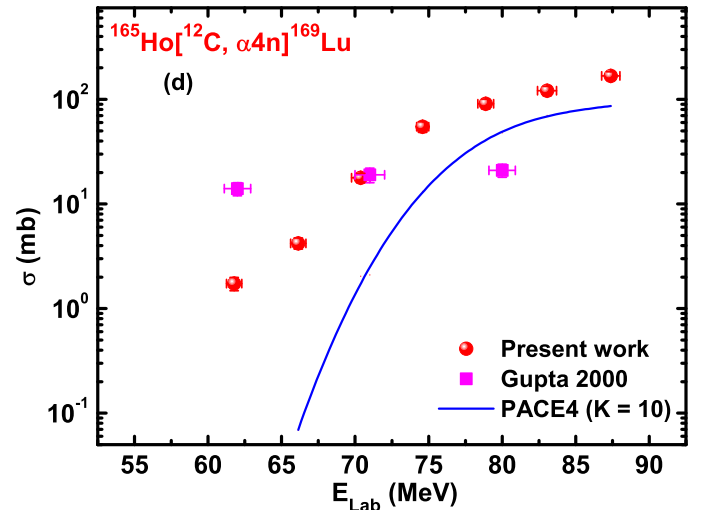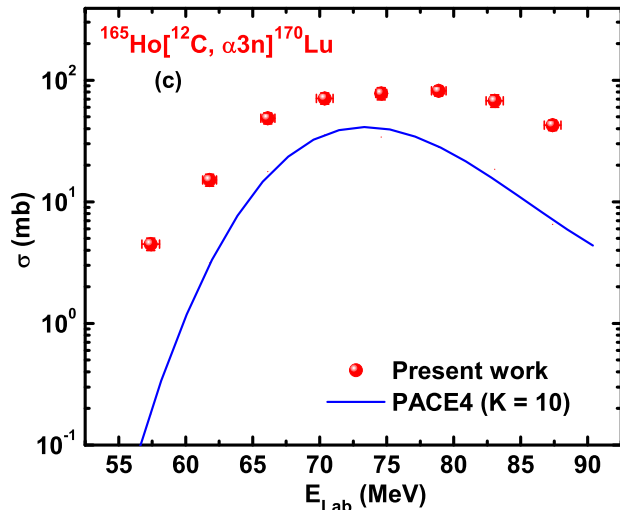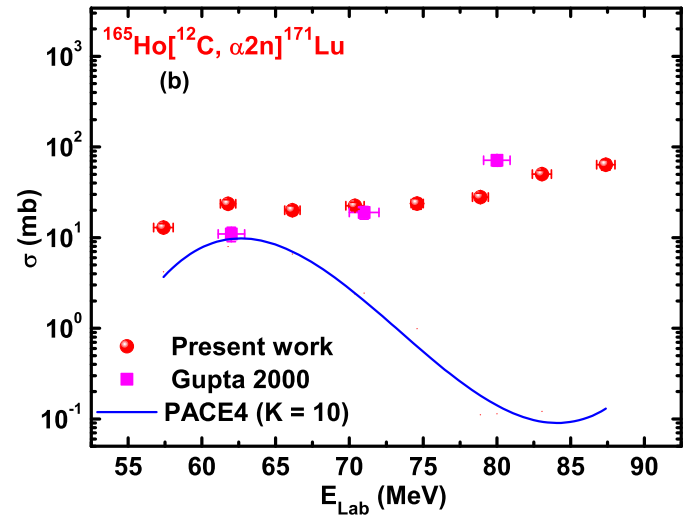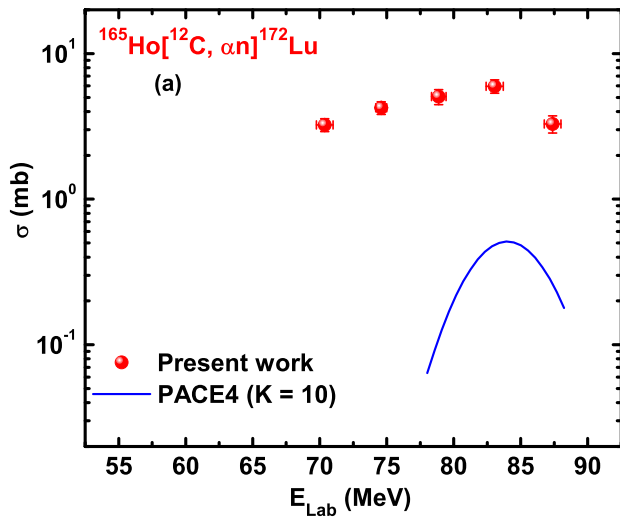

FIG. 6. Experimentally measured EFs of ERs ^{172}Lu (αn), ^{171}Lu (α2n), ^{170}Lu (α3n), and ^{169}Lu (α4n) populated in the interactions of ^{12}C + ^{165}Ho system. The solid lines correspond to the theoretical predictions by statistical model code PACE4 at $K = 10$.
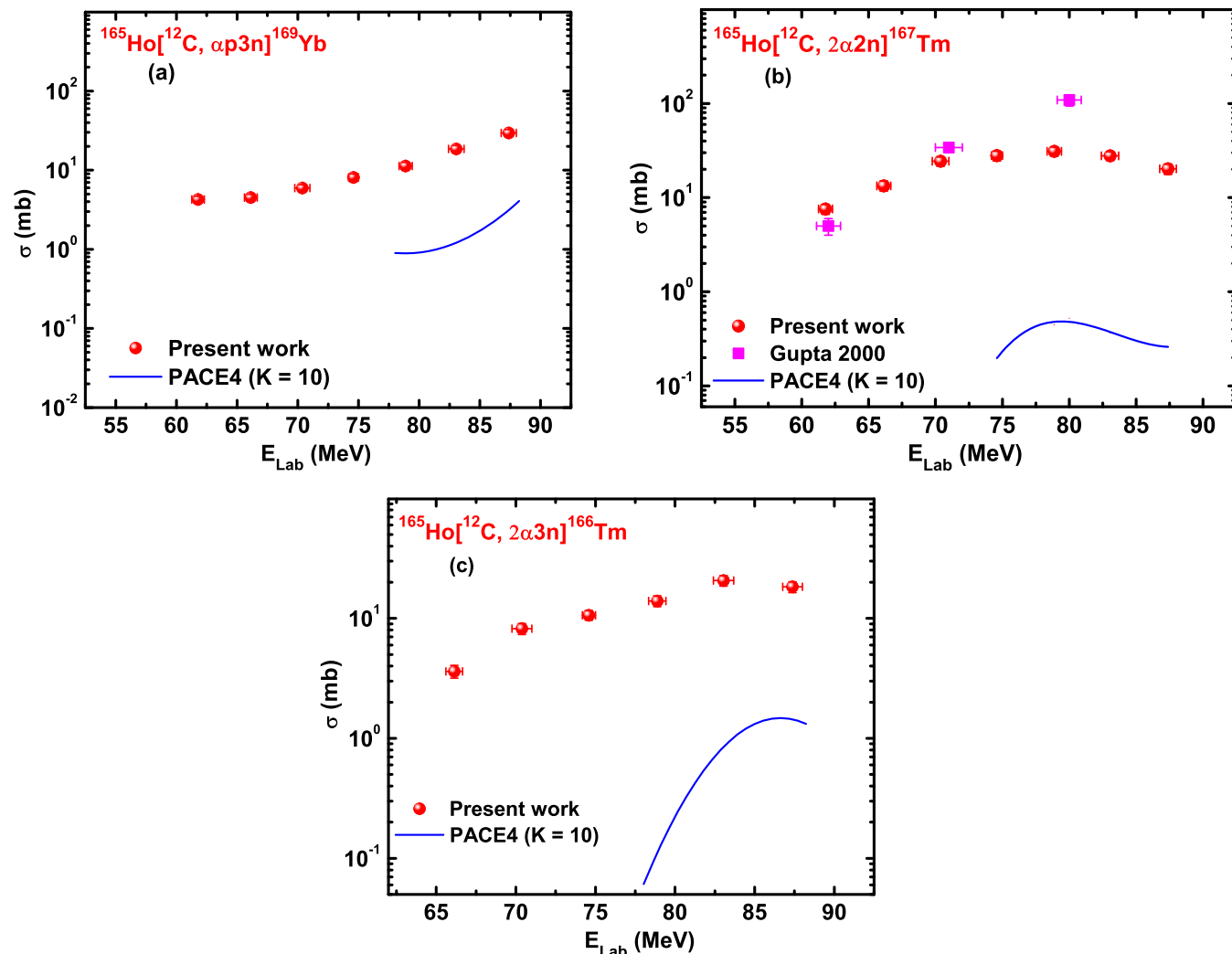
FIG. 7. Experimentally measured EFs of ERs ^{169}Yb ($\alpha p3n$), ^{167}Tm ($2\alpha 2n$), and ^{166}Tm ($2\alpha 3n$) populated in the interactions of ^{12}C + ^{165}Ho system. The solid lines correspond to the theoretical predictions by statistical model code PACE4 at $K = 10$.

ICF channels. Hence, the calculated value of $\Sigma\sigma_{ICF}$ should be treated as lower limit of ICF for the presently studied system which may alter up to small extent by including the missing ICF channels. Furthermore, it is also important to point out that the value of $\Sigma\sigma_{ICF}$ is not pure experimental rather it is partly based on the theoretical prediction of statistical model code PACE4. Thus, the comparisons of various data discussed in the following subsections, where dependence of ICF on the entrance channel parameters and comparison of different data shown are actually not pure comparisons, but are partly based on the theory (PACE4).

A. ICF dependence on the incident projectile energy

In Fig. 8(b), the F_{ICF} (%) calculated for the present system ^{12}C + ^{165}Ho is compared with F_{ICF} (%) deduced for the same system using the data reported in Ref. [12] and plotted against the incident projectile energy. It can be seen from this figure that the F_{ICF} (%) increases with increase in the incident projectile energy; however, the values of F_{ICF} (%) that are derived from Ref. [12] are not in good agreement with

the present measurements. This inconsistency in F_{ICF} (%) is mostly due to the unexpectedly large ICF cross sections of ER ^{165}Tm ($2\alpha 4n$) reported by the authors, which we could not observe in the present work.

Further in Fig. 9, the F_{ICF} (%) obtained for the present system ^{12}C + ^{165}Ho is compared with the F_{ICF} (%) of the other systems namely, ^{13}C + ^{165}Ho [5], ^{16}O + ^{165}Ho [13], ^{20}Ne + ^{165}Ho [10], and plotted against the relative velocity (V_{rel}). The relative velocity of the nucleons in the compound system has been used as a normalization factor to compare the ICF fraction of various systems. For the present system, the F_{ICF} (%) is found to be $\approx 5\%$ at energy 7% above the barrier and increases up to $\approx 16\%$ at energy around 64% above the Coulomb barrier. Similarly, the F_{ICF} (%) for other systems also increases with increase in the incident projectile energy. This increment in F_{ICF} is possibly due to the large angular momentum transmitted to the system, which consequently leads to the fading of fusion pocket in the effective potential energy curve. Hence, to reinstate the fusion pocket and to equip the sustainable input angular momenta for fusion to occur, the projectile break-up probability increases with increase
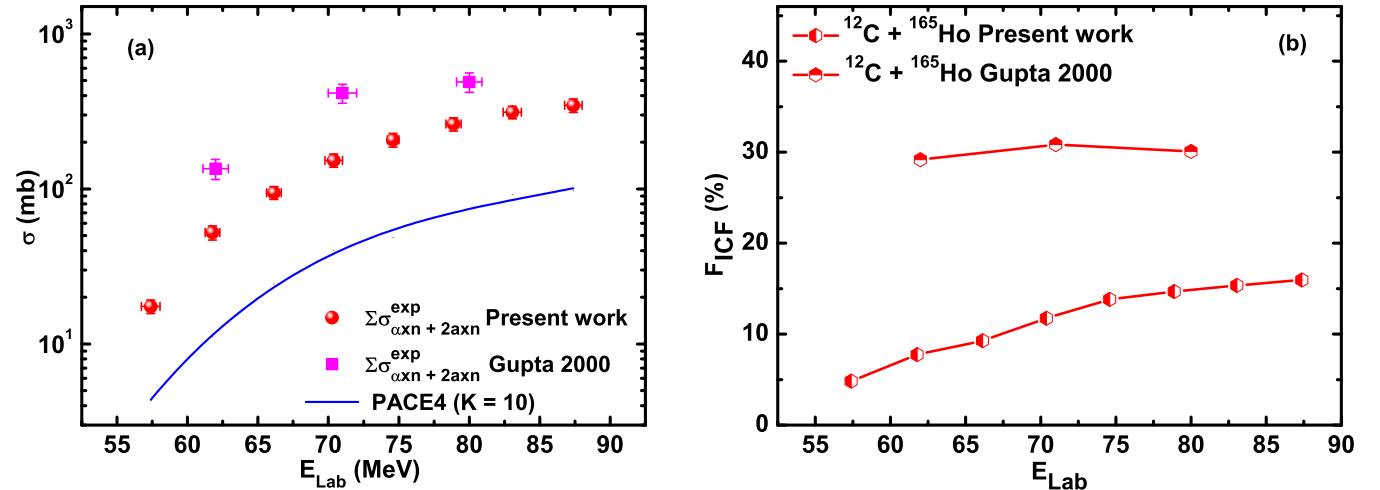
FIG. 8. (a) Comparison of experimentally measured independent cross sections of all $\alpha xn + \alpha pxn + 2\alpha xn$ emission channels $(\sum \sigma_{\alpha xn + \alpha pxn + 2\alpha xn}^{\exp})$ with PACE4 predictions $(\sum \sigma_{\alpha xn + \alpha pxn + 2\alpha xn}^{\text{PACE4}})$ at $K = 10$. (b) The deduced F_{ICF} (%) for ^{12}C + ^{165}Ho system plotted against E_{Lab}.

in the incident projectile energy, hence in turn ICF increases. Moreover, it can be observed from Fig. 9, that for nearly the same value of relative velocity, the order of magnitude of F_{ICF} (%) is less for ^{13}C (non α-cluster structure) than for ^{12}C, ^{16}O, and ^{20}Ne (α-cluster structure) projectile-induced reactions with the same target ^{165}Ho. This implies that in addition to the incident projectile beam energy, some other entrance channel parameters also govern the ICF process.

B. ICF dependence on the mass asymmetry

To understand the ICF sensitivity towards the entrance channel mass asymmetry [$\mu_m = A_T/(A_P + A_T)$] and to understand the validity of mass asymmetry systematic proposed by Morgenstern *et al.* [24], according to whom, systems that are more mass asymmetric contribute remarkably to ICF.
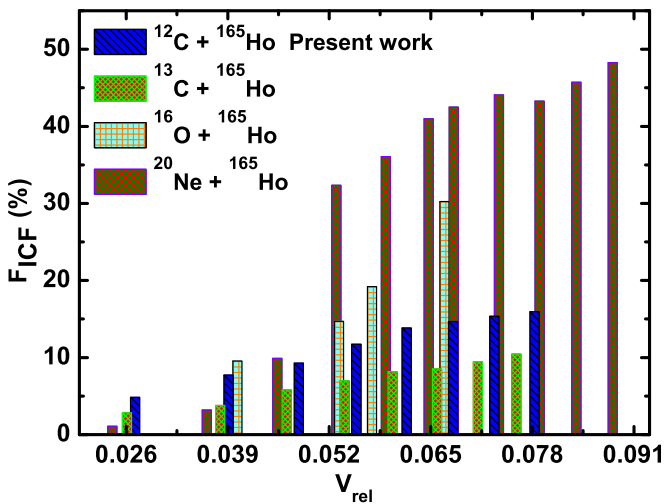
Thus, the deduced ICF fraction (F_{ICF}) for the present system ^{12}C + ^{165}Ho has been compared with those obtained for ^{12}C-induced reactions with ^{103}Rh [25], ^{115}In [26], ^{159}Tb [27], ^{165}Ho [12], ^{169}Tm [28], ^{175}Lu [8], and ^{181}Ta [29] targets, ^{13}C-induced reactions with ^{159}Tb [30], ^{165}Ho [5], ^{169}Tm [31], ^{175}Lu [8], and ^{181}Ta [29] targets, ^{16}O-induced reactions with ^{93}Nb [32], ^{103}Rh [33], ^{115}In [6], ^{130}Te [34], ^{159}Tb [35], ^{165}Ho [13], ^{169}Tm [36], and ^{175}Lu [37] targets, ^{18}O-induced reactions with ^{159}Tb [38] and ^{175}Lu [37] targets and ^{20}Ne + ^{165}Ho [10] system at the same relative velocity ($V_{\text{rel}} \approx 0.053c$) as a function of μ_m and shown in Fig. 10. An interesting trend is
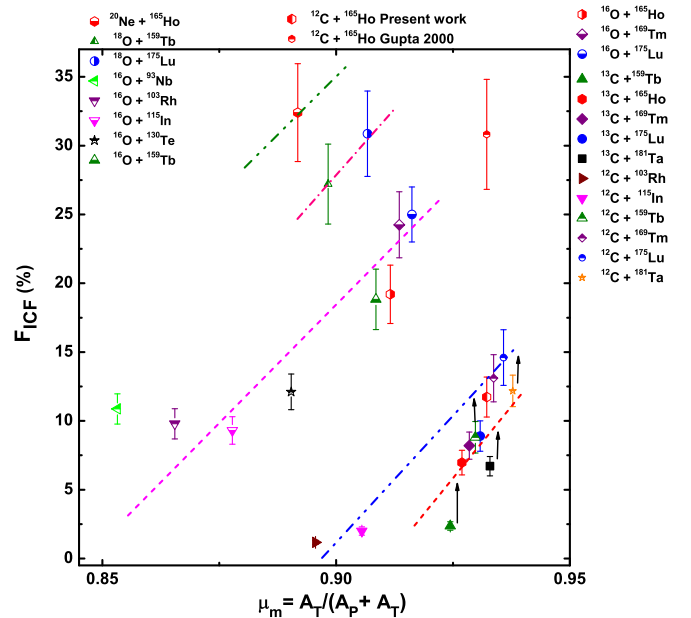

FIG. 9. The comparison of deduced F_{ICF} (%) as a function of relative velocity (V_{rel}) for different projectiles on the same target ^{165}Ho. For references and details see text.

FIG. 10. Comparison of deduced F_{ICF} (%) of ^{12}C + ^{165}Ho system with earlier studied systems as a function of entrance channel mass-asymmetry (μ_m) at same relative velocity ($V_{\text{rel}} \approx 0.053c$). The lines drawn are just to guide the eye. For references and details see text.

observed from this figure, the ICF fraction increases linearly with increase in the mass asymmetry of the systems but separately for each projectile (^{12}C, ^{13}C, ^{16}O, ^{18}O, and ^{20}Ne)-induced reactions with different targets. Another significant observation evident from this figure is, for those projectile-target combinations with nearly the same mass asymmetry like ^{12}C + ^{115}In ($\mu_m = 0.9055$), ^{16}O + ^{159}Tb ($\mu_m = 0.9086$), and ^{18}O + ^{175}Lu ($\mu_m = 0.9067$) the values of ICF fraction are $\approx$2%, 19%, and 31%, respectively. The present observations show a disparity from the systematic proposed by Morgenstern *et al.* [24], where a simple linear growth in ICF fraction with mass asymmetry was suggested. It may be inferred from the present results that mass asymmetry, projectile structure and Coulomb effect ($Z_P Z_T$) of the interacting nuclei govern ICF dependence on mass asymmetry systematic in the concerned energy region. Further the present results are also in good agreement with our recent observations [2,5]. The observed projectile structure effect using α and non α-cluster structured projectiles are elucidated in terms of alpha separation energy or projectile Q_α value in a detailed manner in the subsection D of this manuscript.

C. ICF dependence on Coulomb effect ($Z_P Z_T$)

In the previous subsections, we observed the behavior of ICF with the incident projectile energy and the projectile-target mass asymmetry systematic. To understand the sensitivity of ICF towards the product of projectile charge (Z_P) and target charge (Z_T) i.e., Coulomb effect ($Z_P Z_T$), the deduced F_{ICF} (%) has been plotted at same relative velocity ($V_{rel} \approx 0.053c$) against the $Z_P Z_T$ in Fig. 11. The systems and their symbols are the same as that in Fig. 10. It may be observed from this figure that with increase in the charge product ($Z_P Z_T$) of interacting nuclei, the ICF fraction also increases. This implies that as the incident projectile comes towards the target nucleus the Coulomb repulsion increases, due to which the incident projectile breaks-up into its constituents. This breakup is followed by the fusion of one or more fragments with the target nucleus. More the value of $Z_P Z_T$ in the interacting nuclei, larger is the probability that projectile may break-up and hence in turn larger is the ICF fraction. Further, as mentioned in subsection B, the systems ^{12}C + ^{115}In ($Z_P Z_T = 294$), ^{16}O + ^{159}Tb ($Z_P Z_T = 520$), and ^{18}O + ^{175}Lu ($Z_P Z_T = 568$) have nearly the same mass asymmetry but have significantly different ICF fractions, which could not be explained on the basis of mass asymmetry systematic. This discrepancy may again be efficiently explained on the basis of Coulomb effect. Since the $Z_P Z_T$ value for ^{12}C + ^{115}In < ^{16}O + ^{159}Tb < ^{18}O + ^{175}Lu, hence the magnitude of their ICF fraction also follow the same order.

Moreover, it is quite interesting to see that the F_{ICF} values for ^{12}C, ^{16}O, and ^{20}Ne (α-cluster structured) projectile-induced reactions follow a linear growth in ICF and lie on the same line. However, for ^{13}C and ^{18}O (non-α-cluster structured) projectile-induced reactions, which have the same $Z_P Z_T$ values as that for ^{12}C- and ^{16}O-induced reactions the F_{ICF} values are significantly different. The present observations reveal that the Coulomb effect ($Z_P Z_T$) govern the ICF
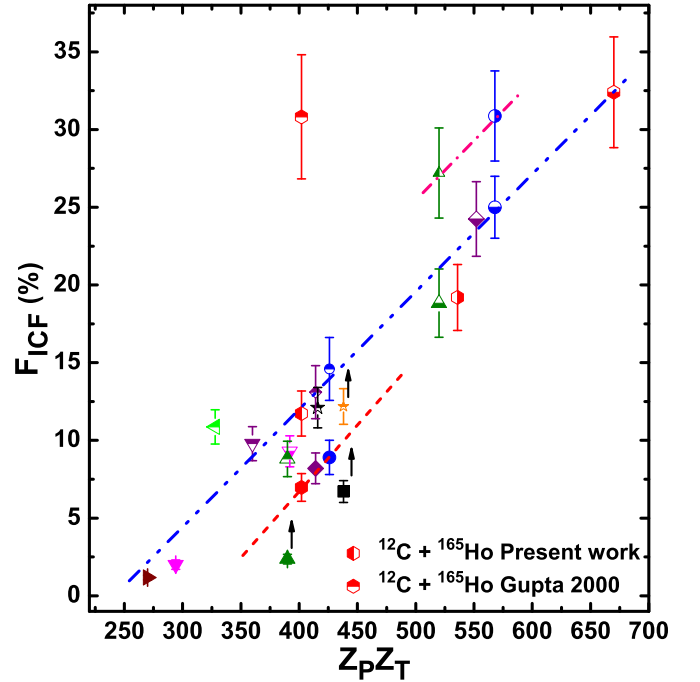

FIG. 11. Comparison of deduced F_{ICF} (%) of ^{12}C + ^{165}Ho system with earlier studied systems as a function of Coulomb effect ($Z_P Z_T$) at same relative velocity ($V_{rel} \approx 0.053c$). The systems and their symbols are the same as that in Fig. 10. The lines drawn are just to guide the eye. For references and details see text.

probability up to some extent and is unaccountable to explain the ICF dynamics for the projectile-target combinations with the same values of $Z_P Z_T$. This inconsistency may again be explained on the basis of projectile Q_α value. In Table IV, a list of projectile-target combinations with the same $Z_P Z_T$ values are given.

TABLE IV. List of projectile-target combinations along with the values of their entrance channel parameter mass asymmetry (μ_m) and Coulomb effect ($Z_P Z_T$).

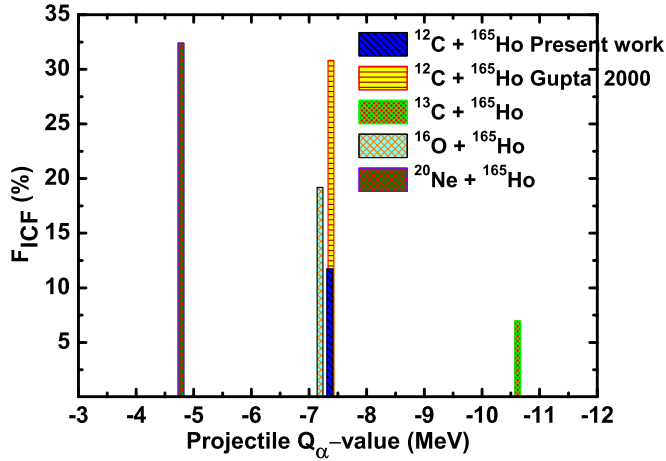| System	μ_m	$Z_P Z_T$	Ref.
^{12}C + ^{159}Tb	0.9298	390	[27]
^{13}C + ^{159}Tb	0.9244	390	[30]
^{12}C + ^{165}Ho	0.9322	402	[12];[a]
^{13}C + ^{165}Ho	0.9269	402	[5]
^{12}C + ^{169}Tm	0.9337	414	[28]
^{13}C + ^{169}Tm	0.9285	414	[31]
^{12}C + ^{175}Lu	0.9358	426	[8]
^{13}C + ^{175}Lu	0.9308	426	[8]
^{12}C + ^{181}Ta	0.9378	438	[29]
^{13}C + ^{181}Ta	0.9329	438	[29]
^{16}O + ^{159}Tb	0.9086	520	[35]
^{18}O + ^{159}Tb	0.8983	520	[38]
^{16}O + ^{175}Lu	0.9162	568	[37]
^{18}O + ^{175}Lu	0.9067	568	[37]

[a]Present work.

FIG. 12. Comparison of F_{ICF} (%) in terms of projectile Q_α value at same relative velocity ($V_{rel} \approx 0.053c$) for ^{12}C, ^{13}C, ^{16}O, and ^{20}Ne projectiles with the same ^{165}Ho target. For references and details see text.

FIG. 13. Comparison of deduced F_{ICF} (%) for ^{12}C + ^{165}Ho (Present work) and ^{18}O + ^{159}Tb [38] systems against the relative velocity. For details see text.

D. ICF dependence on projectile Q_α value

The different magnitudes of ICF fractions in ^{20}Ne-, ^{16}O-, ^{12}C-, and ^{13}C-induced reactions with the same target ^{165}Ho, as observed from Fig. 9, suggests the strong influence of the projectile structure. Further the distinct rates of growth of ICF fraction with mass asymmetry for various projectile-induced reactions with similar or dissimilar targets also indicate toward the role of projectile structure. This projectile structure effect may be understood in terms of projectile Q_α value. The projectile Q_α value simply determines the amount of energy required in separating the alpha particle from the projectile, this is also termed as projectile α-separation energy. In Fig. 12, the ICF fraction calculated for the present system ^{12}C + ^{165}Ho has been compared with the earlier studied systems ^{20}Ne + ^{165}Ho [10], ^{16}O + ^{165}Ho [13], ^{12}C + ^{165}Ho [12], and ^{13}C + ^{165}Ho [5] and plotted against the projectile Q_α value at same relative velocity $0.053c$. The Q_α value for projectiles ^{20}Ne, ^{16}O, ^{12}C, and ^{13}C are as follows:

$$^{20}\text{Ne} \Rightarrow {}^{16}\text{O} + \alpha, \quad Q_\alpha = -4.73 \, \text{MeV},$$
$$^{16}\text{O} \Rightarrow {}^{12}\text{C} + \alpha, \quad Q_\alpha = -7.16 \, \text{MeV},$$
$$^{12}\text{C} \Rightarrow {}^{8}\text{Be} + \alpha, \quad Q_\alpha = -7.37 \, \text{MeV},$$
$$^{13}\text{C} \Rightarrow {}^{9}\text{Be} + \alpha, \quad Q_\alpha = -10.65 \, \text{MeV}.$$

It is apparent from this figure that ^{20}Ne with low Q_α value shows large ICF fraction and subsequently decreases for ^{16}O-, ^{12}C-, and ^{13}C-induced reactions as the Q_α value of the projectile increases. This implies that lower the Q_α value of the projectile higher is its break-up probability in the vicinity of target nuclear field and vice versa. Thus, projectile Q_α value seems to be an important entrance channel parameter, which explains the projectile structure effect more effectively. Moreover, the ICF fraction calculated from the work of Ref. [12] does not follow any of the systematic (mass asymmetry, Coulomb effect, or projectile Q_α value).
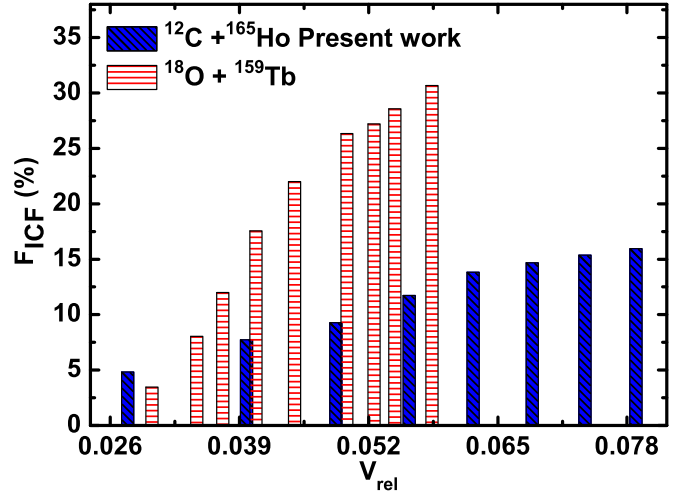
E. Comparison of ICF fraction for same compound nucleus

Both the nuclear interactions ^{12}C + ^{165}Ho (present work) and ^{18}O + ^{159}Tb [38] give rise to the same compound nucleus (CN) ^{177}Ta. To understand how the ICF fraction varies when the two different systems lead to the same CN and to comprehend the role of entrance channel parameters, the ICF fraction deduced for the present work has been compared with the Ref. [38] and plotted against the relative velocity in Fig. 13. It may be seen from this graph that the ICF fraction increases for both the systems with increase in the incident projectile energy but for more mass asymmetric system ^{12}C + ^{165}Ho ($\mu_m = 0.9322$), the F_{ICF} (%) is smaller compared to less mass asymmetric system ^{18}O + ^{159}Tb ($\mu_m = 0.8983$). This inconsistency may be understood on the basis of the Coulomb effect. The $Z_P Z_T$ values for ^{12}C + ^{165}Ho and ^{18}O + ^{159}Tb systems are 402 and 520, respectively, which implies that in the case of a low $Z_P Z_T$ value system, the incident projectile will face less Coulomb repulsion than a higher $Z_P Z_T$ value system. Hence, ICF fraction is smaller in the former than later.

From all these systematic observations we may conclude that a single entrance channel parameter does not govern the ICF reaction dynamics, but have varying contributions depending upon the projectile-target combination. Further, to have more clear understanding we need to perform more experiments which will cover lower-, middle-, as well as higher-mass regions.

F. Universal fusion function: Effect of projectile break-up on complete fusion cross sections

Various reduction methods have been implemented earlier to remove the geometrical factors such as radii and the barrier heights and the static effects of potential between two interacting nuclei to reduce the fusion data. These methods were found to be imprecise and in the new method proposed in Refs. [14,15] proper care has been taken to avoid the limitations of the earlier reduction procedures. In this newly
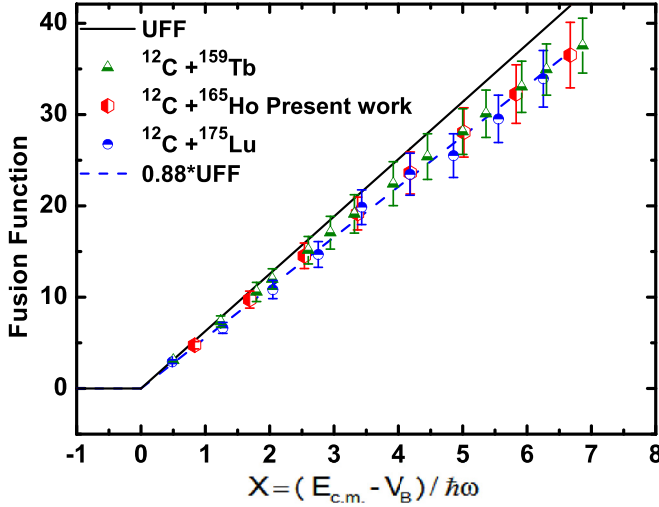
FIG. 14. The complete fusion function $F(x)$ for the α-cluster projectile ^{12}C on different target nuclei as a function of "x." The solid line denotes the UFF and the dotted line represents the UFF multiplied by the suppression factor $F_{B.U.} = 0.88$. For references and details see text.

FIG. 15. The complete fusion function $F(x)$ for the non-α-cluster projectile ^{13}C on different target nuclei as a function of "x." The solid line denotes the UFF and the dotted line represents the UFF multiplied by the suppression factor $F_{B.U.} = 0.93$. For references and details see text.

proposed method, the collision energy and fusion cross section are reduced as under

$$E_{c.m.} \rightarrow x = \frac{E_{c.m.} - V_B}{\hbar\omega}, \quad \sigma_F \rightarrow F(x) = \frac{2E_{c.m.}}{\hbar\omega R_B^2}\sigma_F, \quad (7)$$

where, $E_{c.m.}$ denotes the collision energy in the center of mass frame and σ_F represents the fusion cross section, R_B, V_B, and $\hbar\omega$ is the radius, height, and curvature of the barrier, respectively. This reduction method of Eq. (7) is motivated by Wong's formula for fusion cross section [39]:

$$\sigma_F^W(E_{c.m.}) = \frac{R_B^2\hbar\omega}{2E_{c.m.}} \ln\left[1 + \exp\left(\frac{2\pi(E_{c.m.} - V_B)}{\hbar\omega}\right)\right]. \quad (8)$$

For the projectile-target combinations, if the fusion cross section is correctly described by the Wong's formula, then fusion function $F(x)$ reduces to

$$F_o(x) = \ln[1 + \exp(2\pi x)]. \quad (9)$$

Since, $F_o(x)$ is the general function of dimensionless variable "x" and independent of the projectile-target combination (system), hence it is termed as the universal fusion function (UFF). It allows comparing the fusion cross sections of various projectile-target combinations with distinct Coulomb barriers and any deviation from the UFF is attributed to the projectile break-up effects on CF cross sections. It is important to mention that at energies above the Coulomb barrier the coupling effects other than the projectile break-up do not play any important role on fusion cross sections [40,41]. Keeping this in view, we investigated the influence of projectile break-up effects on CF cross sections at projectile energies above the Coulomb barrier using this reduction procedure. In Fig. 14 the fusion function F(x) for the α-cluster projectile ^{12}C with different targets namely ^{159}Tb [27], ^{165}Ho (present work) and ^{175}Lu [8] as a function of dimensionless variable "x" is
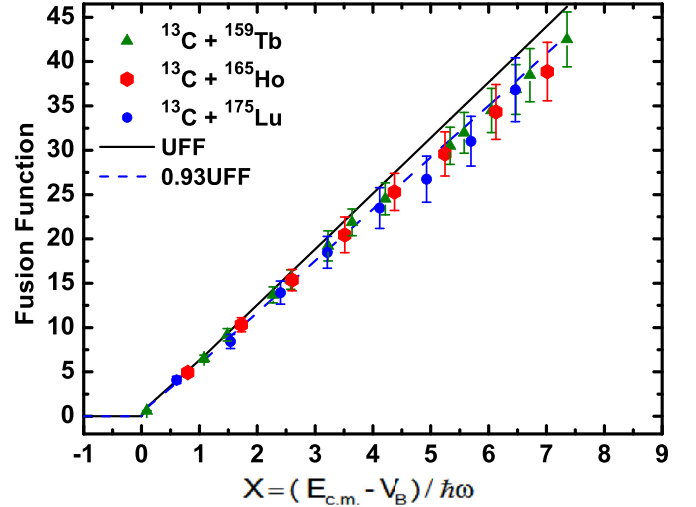
shown. For ^{12}C projectile the most favorable break-up channel is $^{12}C \rightarrow {}^{8}Be + \alpha$ with the threshold energy 7.37 MeV. The UFF, i.e., $F_o(x)$ given in Eq. (9) is represented by the solid line. It can be seen from Fig. 14, at energies above the Coulomb barrier the CF functions are below the UFF for all the three systems. This infers that compared to UFF, CF cross sections are suppressed above the Coulomb barrier energies. This suppression in fusion cross section is attributed to the break-up of ^{12}C projectile into its fragments owing to its low break-up threshold energy.

Similarly, the CF data for ^{13}C (non α-cluster) projectile with ^{159}Tb [30], ^{165}Ho [5], and ^{175}Lu [8] are also studied and shown in Fig. 15. For the ^{13}C projectile, the most favorable break-up channel is $^{13}C \rightarrow {}^{9}Be + \alpha$ with the threshold energy equal to 10.65 MeV. The CF cross sections are suppressed above the Coulomb barrier energies compared to the UFF owing to the presence of break-up process. Moreover, the dotted line in Figs. 14 and 15 denote the UFF multiplied by the suppression factor $F_{B.U.}$, where $F_{B.U.}$ is defined in Ref. [41] as

$$F_{B.U.} = \frac{F(x)}{F_0(x)}. \quad (10)$$

For ^{12}C and ^{13}C, the values of $F_{B.U.}$ are 0.88 and 0.93, respectively, by making a fit. The suppression factor for ^{12}C is smaller than that of ^{13}C because of lower threshold energy for ^{12}C. This also infers that the suppression factor is sensitive toward the break-up threshold energy of the projectile.

It is important to mention here that recently the EF measurements of $^{16}O + {}^{148}Nd$ system have been carried out by Giri *et al.* [42], in which an attempt has also been made to systematically study the low-energy ICF reaction dynamics. While trying to make out the ICF dependence on various entrance channel parameters, it has been observed that ICF
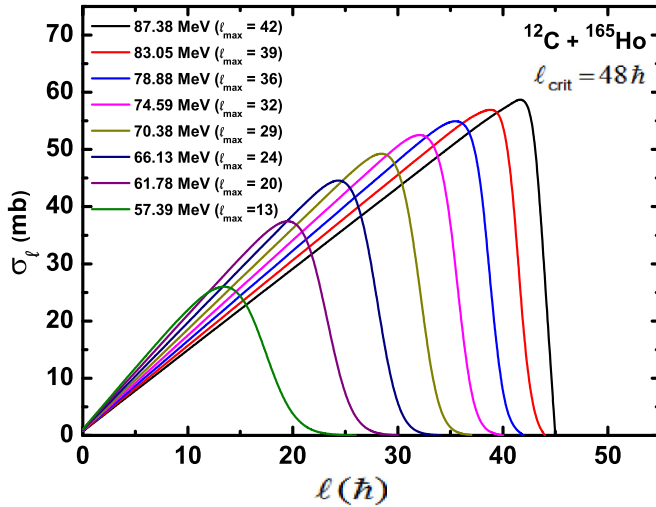
FIG. 16. Fusion ℓ distribution for ^{12}C + ^{165}Ho system calculated using the code CCFULL [44] at the studied energies. For details see text.

also depends on the target deformation (β_2) parameter. Moreover, compared to the linear growth in ICF fraction with the entrance channel parameters such as mass asymmetry, Coulomb effect ($Z_P Z_T$) in the present study, the exponential growth of ICF has been observed with these parameters and interpreted on the basis of target deformation parameter. In addition to this, in the present study comparison of CF cross section with the UFF shows different suppression for ^{12}C- and ^{13}C-induced reactions with the same targets, which evidently suggests the effect of projectile structure, while in the other manuscript [42] this has been explained on the basis of β_2 parameter.

G. Contribution of ICF below critical angular momentum (ℓ_{crit})

According to the SUMRULE model [43], the probability of complete fusion is almost unity below the critical angular momentum (ℓ_{crit}) and the ICF mainly starts contributing for $\ell > \ell_{crit}$, but recently some studies [8,10,44] have reported contribution of ICF below ℓ_{crit} also. Thus, to have the better comprehension of diffuseness in ℓ distribution, the ℓ_{crit} for the ^{12}C + ^{165}Ho (present system) has been calculated using the Wilczynski *et al.* [43] formalism and found to be $48\hbar$. The fusion ℓ distribution for the present studied system is calculated using the code CCFULL [45] at the each studied energy and plotted in Fig. 16. The values of maximum angular momentum ℓ_{max} at the studied energies are found to be in the range of $13\hbar$ to $42\hbar$, which are lower than the ℓ_{crit} for complete fusion for this system. Moreover, the present EF measurements clearly reveal the significant contribution of ICF at the studied energies, this infers that below ℓ_{crit}, there are significant number of ℓ waves which contribute to ICF. The present observations also specify that fusion ℓ

distribution window approached by the SUMRULE model is a broad diffused boundary.

V. SUMMARY AND CONCLUSIONS

In the present work, the EF measurements of thirteen ERs populated in the interaction of ^{12}C + ^{165}Ho system have been studied in the energy region of $\approx$ 4–7 MeV/nucleon. The independent cross sections of some ERs fed by their higher charge precursor isobars have been calculated using the Cavinato *et al.* [18] formalism. The experimentally measured cross sections of the ERs populated via xn and/or pxn channels have been found to agree well with the theoretical predictions of statistical model code PACE4 for level density parameter $a = A/10 \, \text{MeV}^{-1}$, implying the population of these ERs by CF process. However, the experimentally measured cross sections of the ERs populated through α and 2α emission channels show a significant enhancement from the PACE4 prediction even after precursor decay contribution, which is attributed to ICF process. Moreover, the dependence of ICF on various entrance channel parameters has been studied for a large number of projectile-target combinations. It has been observed that every entrance channel parameter plays some significant role in low-energy ICF reaction dynamics. From the mass asymmetry and $Z_P Z_T$ systematic it is, respectively, observed that for the systems with the same value of mass asymmetry and $Z_P Z_T$, the difference in ICF is explained on the basis of Coulomb effect and projectile Q_α value, respectively. It may be concluded that a single entrance channel parameter does not administer the ICF reaction dynamics but have varying contributions depending upon the projectile-target combination. Further to understand the influence of projectile break-up on fusion cross section at projectile energies above the Coulomb barrier, the fusion function $F(x)$ obtained from the CF cross section data for the ^{12,13}C-induced reactions has been compared with the universal fusion function (UFF). A significant CF suppression was observed, which is attributed to the prompt break-up of the projectiles. The lowest break-up threshold of the projectiles determines their suppression factor. Moreover, the present results also infer the existence of ℓ waves below ℓ_{crit}, which contribute to ICF. Furthermore, the results observed in the present work are quite interesting, new, and would be fruitful in comprehending and perfect modeling of ICF reaction dynamics in the energy range of $\approx$ 4–7 MeV/nucleon.

[1] D. Singh, S. B. Linda, P. K. Giri, A. Mahato, R. Tripathi, H. Kumar, M. Afzal Ansari, N. P. M. Sathik, R. Ali, R. Kumar, S. Muralithar, and R. P. Singh, Phys. Lett. B **774**, 7 (2017).

[2] D. Singh, S. B. Linda, P. K. Giri, A. Mahato, R. Tripathi, H. Kumar, S. A. Tali, S. Parashari, A. Ali, R. Dubey, M. Afzal Ansari, R. Kumar, S. Muralithar, and R. P. Singh, Phys. Rev. C **97**, 064610 (2018).

[3] A. Yadav, P. P. Singh, M. Shuaib, V. R. Sharma, I. Bala, Unnati, S. Gupta, D. P. Singh, M. K. Sharma, R. Kumar, S. Muralithar, R. P. Singh, B. P. Singh, and R. Prasad, Phys. Rev. C **96**, 044614 (2017).

[4] C. Gerschel, Nucl. Phys. A **387**, 297 (1982).

[5] S. A. Tali, H. Kumar, M. Afzal Ansari, A. Ali, D. Singh, R. Ali, P. K. Giri, S. B. Linda, S. Parashari, R. Kumar, R. P. Singh, and S. Muralithar, Nucl. Phys. A **970**, 208 (2018).

[6] K. Kumar, T. Ahmad, S. Ali, I. A. Rizvi, A. Agarwal, R. Kumar, and A. K. Chaubey, Phys. Rev. C **88**, 064613 (2013).

[7] H. Tricoire, C. Gerschel, A. Gillibert, and N. Perrin, Z. Phys. A- Atomic Nuclei **323**, 163 (1986).

[8] H. Kumar, S. A. Tali, M. Afzal Ansari, D. Singh, R. Ali, K. Kumar, N. P. M. Sathik, S. Parashari, A. Ali, R. Dubey, I. Bala, R. Kumar, R. P. Singh, and S. Muralithar, Nucl. Phys. A **960**, 53 (2017).

[9] R. Ali, D. Singh, M. Afzal Ansari, M. H. Rashid, R. Guin, and S. K. Das, J. Phys. G, Nucl. Part. Phys. **37**, 115101 (2010).

[10] D. Singh, R. Ali, M. Afzal Ansari, B. S. Tomar, M. H. Rashid, R. Guin, and S. K. Das, Nucl. Phys. A **879**, 107 (2012).

[11] O. B. Tarasov and D. Bazin, NIM B **266**, 4657 (2008); A. Gavron, Phys. Rev. C **21**, 230 (1980); http://lise.nscl.msu.edu/pace4.

[12] S. Gupta, B. P. Singh, M. M. Musthafa, H. D. Bhardwaj, and R. Prasad, Phys. Rev. C **61**, 064613 (2000).

[13] K. Kumar, T. Ahmad, S. Ali, I. A. Rizvi, A. Agarwal, R. Kumar, K. S. Golda, and A. K. Chaubey, Phys. Rev. C **87**, 044608 (2013).

[14] L. F. Canto, P. R. S. Gomes, J. Lubian, L. C. Chamon, and E. Crema, J. Phys. G: Nucl. Part. Phys. **36**, 015109 (2009).

[15] L. F. Canto, P. R. S. Gomes, J. Lubian, L. C. Chamon, and E. Crema, Nucl. Phys. A **821**, 51 (2009).

[16] CANDLE - Collection and Analysis of Nuclear Data using Linux nEtwork; B. P. A. Kumar, E. T. Subramaniam, and R. K. Bhowmik, DAE-BRNS Nucl. Phys. Symp. Kolkata (2001); http://www.iuac.res.in/NIAS/

[17] S. F. Mughabghab, M. Divadeenam, and N. E. Holden, *Neutron Cross-Sections* (Academic Press, New York, 1989), p. 89.

[18] M. Cavinato, E. Fabrici, E. Gadioli, E. Gadioli Erba, P. Vergani, M. Crippa, G. Colombo, I. Redaelli, and M. Ripamonti, Phys. Rev. C **52**, 2577 (1995).

[19] R. Bass, Nucl. Phys. A **231**, 45 (1974).

[20] W. Hauser and H. Feshbach, Phys. Rev. **87**, 366 (1952).

[21] F. D. Becchetti and G. W. Greenlees, Phys. Rev. **182**, 1190 (1969).

[22] A. Gilbert and A. G. W. Cameron, Can. J. Phys. **43**, 1446 (1965).

[23] J. P. Lestone, Phys. Rev. C **53**, 2014 (1996).

[24] H. Morgenstern, W. Bohne, W. Galster, K. Grabisch, and A. Kyanowski, Phys. Rev Lett. **52**, 1104 (1984).

[25] B. B. Kumar, A. Sharma, S. Mukherjee, S. Chakrabarty, P. K. Pujari, B. S. Tomar, A. Goswami, S. B. Manohar, and S. K. Datta, Phys. Rev. C **59**, 2923 (1999).

[26] S. Mukherjee, A. Sharma, S. Sodaye, A. Goswami, and B. S. Tomar, Int. Jour. Mod. Phys. E **15**, 237 (2006).

[27] A. Yadav, V. R. Sharma, P. P. Singh, D. P. Singh, M. K. Sharma, U. Gupta, R. Kumar, B. P. Singh, R. Prasad, and R. K. Bhowmik, Phys. Rev. C **85**, 034614 (2012).

[28] S. Chakrabarty, B. S. Tomar, A. Goswami, G. K. Gubbi, S. B. Manohar, A. Sharma, B. BinduKumar, and S. Mukherjee, Nucl. Phys. A **678**, 355 (2000).

[29] K. S. Babu, R. Tripathi, K. Sudarshan, B. D. Shirvastava, A. Goswami, and B. S. Tomar, J. Phys. G. Nucl. Part. Phys. **29**, 1011 (2003).

[30] A. Yadav, V. R. Sharma, P. P. Singh, R. Kumar, D. P. Singh, Unnati, M. K. Sharma, B. P. Singh, and R. Prasad, Phys. Rev. C **86**, 014603 (2012).

[31] V. R. Sharma, A. Yadav, P. P. Singh, D. P. Singh, S. Gupta, M. K. Sharma, I. Bala, R. Kumar, S. Murlithar, B. P. Singh, and R. Prasad, Phys. Rev. C **89**, 024608 (2014).

[32] A. Sharma, B. B. Kumar, S. Mukherjee, S. Chakrabarty, B. S. Tomar, A. Goswami, and S. B. Manohar, J. Phys. G: Nucl. Part. Phys. **25**, 2289 (1999).

[33] U. Gupta, P. P. Singh, D. P. Singh, M. K. Sharma, A. Yadav, R. Kumar, B. P. Singh, and R. Prasad, Nucl. Phys. A **811**, 77 (2008).

[34] D. P. Singh, V. R. Sharma, A. Yadav, P. P. Singh, Unnati, M. K. Sharma, R. Kumar, B. P. Singh, and R. Prasad, Phys. Rev. C **89**, 024612 (2014).

[35] M. K. Sharma, Unnati, B. P. Singh, R. Kumar, K. S. Golda, H. D. Bhardwaj, and R. Prasad, Nucl. Phys. A **776**, 83 (2006).

[36] P. P. Singh, B. P. Singh, M. K. Sharma, Unnati, D. P. Singh, R. Prasad, R. Kumar, and K. S. Golda, Phys. Rev. C **77**, 014607 (2008).

[37] H. Kumar, Ph.D. thesis, Aligarh Muslim University, 2017.

[38] A. Yadav, M. Shuaib, A. V. Aggarwal, V. R. Sharma, I. Bala, D. P. Singh, P. P. Singh, Unnati, M. K. Sharma, R. Kumar, R. P. Singh, S. Muralithar, B. P. Singh, and R. Prasad, EPJ Web. Conf. **117**, 08022 (2016).

[39] C. Y. Wong, Phys. Rev. Lett. **31**, 766 (1973).

[40] J. R. Leigh, M. Dasgupta, D. J. Hinde, J. C. Mein, C. R. Morton, R. C. Lemmon, J. P. Lestone, J. O. Newton, H. Timmers, J. X. Wei, and N. Rowley, Phys. Rev. C **52**, 3151 (1995).

[41] B. Wang, W.-J. Zhao, P. R. S. Gomes, En-Guang Zhao, and Shan-Gui Zhou, Phys. Rev. C **90**, 034612 (2014).

[42] P. K. Giri, D. Singh, A. Mahato, S. B. Linda, H. Kumar, S. A. Tali, S. Parashari, A. Ali, M. Afzal Ansari, R. Dubey, R. Kumar, S. Muralithar, and R. P. Singh, Phys. Rev. C **100**, 024621 (2019).

[43] J. Wilczynski, K. Siwek-Wilczynska, J. Van-Driel, S. Gonggrijp, D. C. J. M. Hageman, R. V. F. Janssens, J. Lukasiak, R. H. Siemssen, and S. Y. Van Der Werf, Nucl. Phys. A **373**, 109 (1982).

[44] A. Yadav, V. R. Sharma, P. P. Singh, D. P. Singh, R. Kumar, Unnati, M. K. Sharma, B. P. Singh, R. Prasad, and R. K. Bhowmik, Phys. Rev. C **85**, 064617 (2012).

[45] K. Hagino, N. Rowley, and A. T. Kruppa, Comput. Phys. Commun. **123**, 143 (1999).